Thermal Rossby waves in a rotating annulus. Their stability

D. Pino, M. Net, J. Sánchez, and I. Mercader
Departament de Física Aplicada, Universitat Politècnica de Catalunya, Jordi Girona 1-3, Campus Nord, Mòdul B-4, 08034 Barcelona, Spain

(Received 9 August 2000; published 25 April 2001)

Nonlinear thermal convection in a fast rotating annulus about its axis, with slightly inclined ends, radial gravity and heating, is studied numerically for a fluid of Prandtl number $\sigma = 0.7$ and different values of the radius ratio and rotation rate. The properties of the rotating waves that appear after the Hopf bifurcation of the conductive state are analyzed. Near the critical Rayleigh number, different types of solutions with the same wave number coexist, and they are classified as a function of their connection with the two types of modes identified in the linear analysis for this Prandtl number. For different rotation rates, the stability of the primary solutions as a function of the radius ratio is also studied. The shape of the stability regions and the type of dominant disturbances that limit these regions are very sensitive to the proximity to the value of the radius ratio for which the type of dominant mode changes.

DOI: 10.1103/PhysRevE.63.056312 PACS number(s): 47.20.Ft, 47.20.Lz, 47.20.Ky

I. INTRODUCTION

The understanding of thermal convection in rotating spherical Boussinesq fluid shells is the first stage of an extremely ambitious and nowadays impossible project, in which the dynamics in planetary and stellar atmospheres, including other aspects such as variations of the density, radiative transport of the heat, and magnetic-field effects, were analyzed (see the review [1]). In regard to that problem, it is known that the onset of convection is characterized by the presence of different types of modes, depending on the rotation rate and the Prandtl number of the fluid [2]. The asymptotic analysis of the nonaxisymmetric problem for high rotation rates [3], assumes a simple two-dimensional roll-type structure without a significant distortion, known as normal columnar convection [4]. For small Prandtl numbers and low rotation rates, the preferred modes, the so-called equatorially trapped modes, are fast drifting waves consisting of cells attached to the outer boundary at low latitudes. They correspond to inertial convection [5,6]. When the rotation increases, there is a transition to another type of convection, the spiralling columnar modes, which span azimuthally various wavelengths from middle latitudes to the equatorial region [4]. Transition modes between the equatorial-trapped modes and the spiralling columns, exhibiting multihump structure, have been identified recently by Ref. [2] for intermediate values of the rotation rate. Although the onset of convection has been widely studied, this is not the case with the nonlinear problem of finite amplitude convection. Due to the numerical effort that three-dimensional computations require, it has only been partially explored ([4,2,7] among others). For this reason, simplified geometries, providing a description of the dynamics with lesser numerical effort, have been adopted in order to mimic some regions of the full spherical shell.

Thus, the problem of thermal convection in rotating cylindrical annulus has become a prototype for the study of the dynamics in rotating spherical fluid shells as far as the equatorial region is concerned. For sufficiently high rotation rates, the Taylor-Proudman constraint forces the motion to be two dimensional, independent of the coordinate in the direction of the axis of rotation, and then, the assumption of nearly geostrophic solutions can be made [8]. This system therefore admits columnar solutions such as those in the spherical shell. Furthermore, if the end boundaries are not parallel, a Rossby wavelike dynamics must be expected. Much work has been carried out on such a system using the approximation of small gap [8–11]. However, with symmetric boundary conditions at the sidewalls, and ends without curvature, this approximation prevents the appearance of the spiralling columnar modes obtained in spherical shells [5,7].

In our previous paper [12], the onset of convection in a fast rotating annulus with slightly inclined top and bottom lids and radial gravity and heating was studied. In our model, the curvature of the annulus was retained, and the radial dependence was analyzed as a function of the gap. Different Prandtl numbers, representative of large, moderate, and low values were considered. For moderate and high Prandtl numbers, two different families of dominant columnar modes were found: the modes attached to the inner wall and slanted to the prograde direction, and the almost straight modes with convection occupying the entire layer. According to Ref. [4], we will refer to these modes as *spiral* columnar modes and *normal* columnar modes, respectively. For these Prandtl numbers, we showed that the instability is induced by both thermal and rotation effects, and similar to Ref. [8], we called the marginal waves, thermal Rossby modes. For small Prandtl numbers, we found that, independently of the rotation rates analyzed, the dominant modes, which correspond to the inertial solution of the Poincaré equation, were of *normal* columnar type. The linear modes for small Prandtl numbers thus differed substantially from those obtained in spherical shells

The works of Refs. [6,13] analyzed finite amplitude convection in rotating spherical shells in the range of parameters where the linear modes were columnar and for values of the Rayleigh number not very far from the critical value. They found that no matter what the Prandtl number, the meridional circulation is very weak. However, for Prandtl numbers of order unity or less, the differential rotation dominates the

drifting spiralling convection and was nearly independent of the coordinate in the direction of the axis of rotation; whereas for large Prandtl numbers, the flow is dominated by the normal columnar convection with a weak differential rotation strongly dependent on this coordinate, and originated by a thermal wind mechanism [14]. Thus, from these results, and those in Ref. [12], it follows that preference should be given to the annular system for modeling the dynamics in a spherical shell of fluids with Prandtl numbers of order unity.

In this paper, which is a logical continuation of Ref. [12], we consider the same annular configuration, and we are interested in the nonlinear properties of the convection, which will appear in the form of rotating waves after the Hopf bifurcation of the conductive state. All the results are for Prandtl number 0.7. For this value of the Prandtl number, we obtained that small values of the Coriolis parameter and high values of the radius ratio favor the *normal* columnar modes, whereas the *spiral modes* tend to be dominant for high values of the Coriolis parameter and smaller values of the radius ratio. Rotating waves resulting from or related to these two types of modes will be analyzed. The two dimensions of these solutions and their simple temporal dependence allows an analysis of their stability, which has also been carried out.

The remainder of the paper is organized as follows. The basic model equations and the numerical techniques used to calculate the rotating waves, and to analyze their stability are summarized in Sec. II. Section III is divided into two parts. In the first part we focus our attention mainly on two cases representative of the nonlinear solutions that result from both the *normal* and the *spiral* modes, and we describe the nonlinear properties of these waves. In the second part we deal with the stability of the primary solutions. The paper concludes with a discussion in Sec. IV.

II. BASIC EQUATIONS AND NUMERICAL METHOD

We consider a fluid contained in a cylindrical annulus of height $L(r)$ decreasing outwards, rotating about its axis of symmetry with a fast rotation rate Ω, and the tangent of the angle of inclination φ of the lids with respect to the horizontal, γ, being very small ($\gamma \ll 1$). The mean height of the annulus will be denoted by L_0. The gap of the annulus is $D=r_o-r_i$, where r_o and r_i are the outer and inner radius, respectively. The temperatures T_o and T_i ($T_i>T_o$) are kept constant on the outer and inner sidewalls, and the lids are considered thermally insulating. Our model assumes a constant effective radial gravity inwards g_e, obtained from the average of the radial gravity and centrifugal force. The velocity field satisfies nonslip boundary conditions at the sidewalls, and has a vanishing normal component at the lids. As is discussed in detail in Ref. [3], boundary conditions on the tangential components are irrelevant as long as $\sigma \sin\varphi \gg E^{1/4}$ holds, where E is the Ekman number and σ is the Prandtl number defined below.

Since $\gamma \ll 1$, the system admits a basic conductive state

$$T_c(r)=T_i+\Delta T\frac{\ln r/r_i}{\ln \eta}, \quad \mathbf{u}_c=0, \tag{2.1}$$

in the rotating frame of reference of the cylinder, with $\Delta T=T_i-T_o$ and $\eta=r_i/r_o$. The dimensionless Navier-Stokes equations in the Boussinesq approximation, written in the rotating frame of reference, and the heat equation, are given by Eqs. (2.4) of Ref. [12]. The gap width of the layer D, D^2/κ, and ΔT were used as scales for length, time, and temperature, respectively, where κ denotes the thermal diffusivity.

If we require $\gamma \ll 1$ and high rotation rates, previous theoretical and numerical results [8,15,16] justify the assumption of nearly geostrophic solutions. Then, we have assumed the following decomposition

$$\mathbf{u}=f(r,t)\hat{\mathbf{e}}_\theta+\boldsymbol{\nabla}\times[\psi(r,\theta,t)\hat{\mathbf{e}}_z]+\tilde{\mathbf{u}}(r,\theta,z,t), \tag{2.2a}$$

$$T=T_c(r)+\Theta(r,\theta,t)+\tilde{\Theta}(r,\theta,z,t), \tag{2.2b}$$

where the azimuthal average of ψ is null, and $\tilde{\mathbf{u}}(r,\theta,z,t),\tilde{\Theta}(r,\theta,z,t)$ are order γ. So, at leading order in γ, the azimuthal average of u_θ is $f(r,t)$. Equations for f, ψ, and Θ are obtained from the azimuthal average of the θ component of Navier-Stokes equations, the z component of the vorticity equation, and the heat equation, where we neglect terms of the order γ everywhere except in the Coriolis term. Following Ref. [8], if we average these equations over the z interval and take into account the boundary conditions, the equations are written

$$\left(\frac{1}{\sigma}\partial_t-\nabla_-^2\right)f=\frac{1}{\sigma}P_\theta\left[\nabla_h^2\psi\cdot\frac{1}{r}\partial_\theta\psi\right], \tag{2.3a}$$

$$\begin{aligned}\left(\frac{1}{\sigma}\partial_t-\nabla_h^2\right)\nabla_h^2\psi=&\frac{Ra}{r}\partial_\theta\Theta+\tau\frac{1}{r}\partial_\theta\psi\\&+\frac{1}{\sigma r}[\nabla_-^2 f\partial_\theta\psi-f\partial_\theta\nabla_h^2\psi]\\&+\frac{1}{\sigma r}[\partial_\theta\nabla_h^2\psi\partial_r\psi-\partial_r\nabla_h^2\psi\partial_\theta\psi],\end{aligned} \tag{2.3b}$$

$$\begin{aligned}\partial_t\Theta=&\nabla_h^2\Theta-\frac{1}{r^2\ln\eta}\partial_\theta\psi-f\left(\frac{1}{r}\partial_\theta\Theta\right)\\&+\frac{1}{r}[\partial_\theta\Theta\partial_r\psi-\partial_r\Theta\partial_\theta\psi],\end{aligned} \tag{2.3c}$$

where ∇_h^2 denotes the horizontal Laplacian operator $\nabla_h^2\equiv(1/r)\partial_r(r\partial_r)+(1/r^2)\partial_{\theta\theta}^2$, $\nabla_-^2\equiv(1/r)\partial_r(r\partial_r)-(1/r^2)$, and P_θ is the projection operator that extracts the zero azimuthal mode (see Ref. [12] for details). The dimensionless parameters in the above equations are the Rayleigh number Ra, the Prandtl number σ, and the Coriolis parameter τ, defined as

$$\mathrm{Ra}\equiv\frac{\alpha\Delta T g_e D^3}{\kappa\nu}, \quad \sigma\equiv\frac{\nu}{\kappa}, \quad \tau\equiv\frac{4\gamma\Omega D^3}{\nu L_0},$$

where α is the coefficient of thermal expansion and ν is the kinematic viscosity. Similar equations, without the Coriolis term, were used in Ref. [17] to study the nonlinear dynamics of the Taylor columns.

The geometry of the domain implies that ψ and Θ are periodic in θ, and due to the decompositions (2.2a) and (2.2b), as was detailed in Ref. [12], the boundary conditions on r_i and r_o are written

$$f=\Theta=\psi=\partial_r\psi=0. \tag{2.3d}$$

Equations (2.3a), (2.3b), and (2.3c) together with the boundary conditions, possess **SO**(2) symmetry, i.e., they are invariant under rotations

$$R_{\theta_0}:(r,\theta)\to(r,\theta+\theta_0),\quad (f,\psi,\Theta)\to(f,\psi,\Theta).$$

Other authors have analyzed the same problem, but using the small gap approximation [10]. In the limit of the small gap width, a plane layer approximation can be used. If we denote by y and x the azimuthal and radial coordinates, respectively, defined relative to the midplane, the resulting system will have the translation symmetry in the y direction T_l and an additional symmetry not possessed by equations (2.3a), (2.3b), (2.3c), and (2.3d). They are invariant under the reflection

$$\kappa:(x,y)\to(-x,y),\quad (f,\psi,\Theta)\to(f,-\psi,-\Theta).$$

As a consequence of this reflection symmetry, the symmetry group of the problem in the small-gap approximation is the group $\Gamma=\mathbf{SO}(2)\times\mathbf{Z}_2$. In this problem, when perturbations of wave number α are considered, the Hopf bifurcation of the conductive state leads to primary solutions, which are rotating waves of wavelength $a=2\pi/\alpha$. For the values of the Coriolis parameter τ considered in this paper, and for the critical value of $\alpha=\alpha_c$, these periodic solutions possess a symmetry that is an element $(\kappa,t_0)\in\Gamma\times\mathbf{S}^1$, such that the spatial action of κ is exactly compensated by a phase shift $t_0=\mathcal{T}/2$, where $\mathcal{T}$ is the period of the solutions. So, the rotating waves are invariant under the *shift-reflect* operation $T_{a/2}\kappa$. These solutions have been called *symmetric thermal Rossby waves* in the works of Busse and collaborators ([9,10] among others).

Notice that, if instead of Eq. (2.2a), the decomposition of the velocity field $\mathbf{u}=\boldsymbol{\nabla}\times[\chi(r,\theta,t)\hat{\mathbf{e}}_z]+\tilde{\mathbf{u}}(r,\theta,z,t)$ is used, it is necessary to introduce an additional boundary condition that ensures the periodicity of the pressure gradient in the azimuthal direction (see Ref. [18] for a general discussion). The correct boundary conditions for the small-gap approximation of the problem with rigid sidewalls are given in Ref. [19]. Another recognized problem in which a similar boundary condition is needed is the two-dimensional Poiseuille problem with constant average pressure gradient parametrization, when a stream function formulation is used. The additional boundary condition for this case is discussed in Refs. [20] and [21].

As a measure of the heat transport by convection, we will use the Nusselt number Nu evaluated at the outer cylindrical surface, which has the following expression

$$\mathrm{Nu}=1+\frac{1}{1-\eta}\ln\eta\,\partial_r\langle\Theta\rangle_{r_o},$$

where the symbol $\langle\,\rangle_{r_o}$ denotes the average over the outer surface. To characterize the contribution of the mean zonal flow f over the velocity field, we will introduce the ratio r_f of the kinetic energy E_f associated to f, to the total kinetic energy E_t,

$$r_f=\frac{\langle E_f\rangle}{\langle E_t\rangle},$$

where the symbol $\langle\,\rangle$ now represents the average over the annulus fluid shell.

It is known that the primary convective solutions have the form of rotating waves in the rotating frame of reference of the cylinder. To obtain a solution of this type, we have expanded f, ψ, and Θ in terms of complete systems of functions,

$$f(r,t)=\sum_{j=2}^{J}a_j p_j(x), \tag{2.4a}$$

$$\psi(r,\theta,t)=\sum_{n=1}^{N}\sum_{j=4}^{J}b_{n,j}\exp[inM(\theta-\omega t)]h_j(x)+\text{c.c.}, \tag{2.4b}$$

$$\Theta(r,\theta,t)=\sum_{n=0}^{N}\sum_{j=2}^{J}c_{n,j}\exp[inM(\theta-\omega t)]p_j(x)+\text{c.c.}, \tag{2.4c}$$

where x is related to the radial coordinate r as $x=2r-(1+\eta)/(1-\eta)$, M is the wave number, ω is the drift rate of the wave, prograde if $\omega>0$ and retrograde if $\omega<0$, and a_j, $b_{n,j}$, and $c_{n,j}$ are time independent coefficients, the latter two being complex. The functions $h_j(x)$ and $p_j(x)$, specified in Ref. [12], are linear combinations of the Tchebyshev polynomials satisfying the radial boundary conditions.

Letting $\tilde{\theta}=\theta-\omega t$, we obtain from Eqs. (2.3a), (2.3b), and (2.3c) a set of steady equations, which have been solved numerically using a spectral Galerkin-Fourier technique in $\tilde{\theta}$ and a collocation method in x. Because of the rotation invariance, we have fixed the phase of the solution by prescribing a relation between some coefficients and using the corresponding equation to determine ω. For particular values of the Prandtl number σ, the Coriolis parameter τ, and radius ratio η, a continuation procedure has been used for the location of the equilibria solutions to study their dependence with respect to the Rayleigh number. The curves of solutions have been obtained using a predictor-corrector continuation algorithm (see Ref. [22] for details).

Similar to Ref. [21], the stability of a rotating wave of wave number M has been analyzed by superposing onto it infinitesimal perturbations of the form

$$\psi_m^*(r,\tilde{\theta},t)=\sum_{n=-N}^{N}\sum_{j=4}^{J} b_{n,j}^*\exp[i(n+d_m)M\tilde{\theta}]h_j(x)e^{\lambda_m t}, \tag{2.5a}$$

$$\Theta_m^*(r,\tilde{\theta},t)=\sum_{n=-N}^{N}\sum_{j=2}^{J} c_{n,j}^*\exp[i(n+d_m)M\tilde{\theta}]p_j(x)e^{\lambda_m t}, \tag{2.5b}$$

where $d_m=m/M$ (m is an integer that varies between 0 and $M-1$), and solving the corresponding eigenvalue problem for every value of m. If $m=0$, it is necessary to eliminate from the expansion of the perturbation ψ_0^* the term corresponding to the index $n=0$, and to add

$$f^*(r,t)=\sum_{j=2}^{J} a_j^* p_j(x)e^{\lambda_0 t}. \tag{2.5c}$$

If for some value of m, the real part of λ_m is positive, the M-periodic drifting wave is unstable, otherwise it is stable. When some λ_m crosses the imaginary axis, a bifurcation occurs.

The case $m=0$ corresponds to perturbations with the same wave number as the basic flow, and we will refer to them as superharmonic perturbations. In this case, we always obtain a zero eigenvalue corresponding to the trivial phase-shift solution; an additional zero eigenvalue indicates a saddle-node bifurcation.

For the case $m\neq 0$, since the linear operator describing the stability problem is real, the eigenfunctions for the problem with d_{M-m} can be obtained by conjugating those with d_m; moreover λ_{M-m} is the complex conjugate of λ_m. Then, to analyze the stability properties and bifurcations of the steadily drifting waves, it suffices to consider perturbations with $m\in[1,M/2]$ if M is even, and with $m\in[1,(M-1)/2]$ if it is odd. We will refer to these types of perturbations as subharmonic perturbations. Notice that if a M-periodic drifting solution with drift rate ω suffers a bifurcation of this type $[\Re(\lambda_m)=0]$, additional wave numbers $k_n=nM+m$ and $k_n'=(n+1)M-m$ are excited at linear order in the bifurcated solution, the corresponding frequencies being $\omega_n=k_n\omega-\Im(\lambda_m)$ and $\omega_n'=k_n'\omega+\Im(\lambda_m)$. Then, in a bifurcation of this type, the basic wave periodicity $2\pi/M$ is broken and a new solution with a larger period emerges. At large amplitude, the basic wave number of the bifurcated solution is the greatest common divisor of m and M.

In the range of parameters studied, and for the Prandtl number considered $\sigma=0.7$, a resolution of $N=8$ and $J=24$ suffices to give more than three significant figures in the values of the Nusselt number, and in the drift rate of the rotating waves. The same resolution gives more than five significant figures for the value of the Rayleigh number, and more than four for the $\Im(\lambda_m)$ at the points where a bifurcation occurs.

III. RESULTS

In this section, we present the results, for values of the Rayleigh number near the onset of convection, corresponding to the analysis of the nonlinear dynamics associated to the two types of modes, *normal* and *spiral*, identified in the linear stability analysis of the conductive state [12] for a fluid of Prandtl number $\sigma=0.7$. The range of parameters considered is the same as in our previous paper [12], and covers values of the Coriolis parameter, τ, between 2000 and 11 000 and radius ratios $\eta>0.1$. Our results in the quoted paper show that for fixed values of τ, the *spiral* modes are preferred for small radius ratios. However, for $\eta>0.15$ and $\tau>2300$, it was found that there always exists a value of the radius ratio, η_c, from which the preferred mode is *normal*, according to the results of the problem in the small-gap approximation. The higher the Coriolis parameter τ is, the higher the value η_c is. Thus, in Fig. 1, where we present for $\tau=8000$ the marginal curve of the conductive state as a function of the radius ratio, the value of η_c is 0.605. To illustrate the patterns associated to the two families of modes, the streamlines in the rotating frame of reference of the cylinder of two nonlinear solutions, are shown in this figure. These solutions come from the preferred modes of the linear problem at the radius ratios $\eta=0.35$ (*spiral*) and $\eta=0.7$ (*normal*), the corresponding wave numbers being $M=10$ and $M=37$, respectively. Since the Rayleigh number $\mathrm{Ra}=100\,000$ of these solutions is near the critical value at every η, these streamlines resemble those of the linear modes. All the streamlines plotted in the figures of this paper correspond to the contour plots of

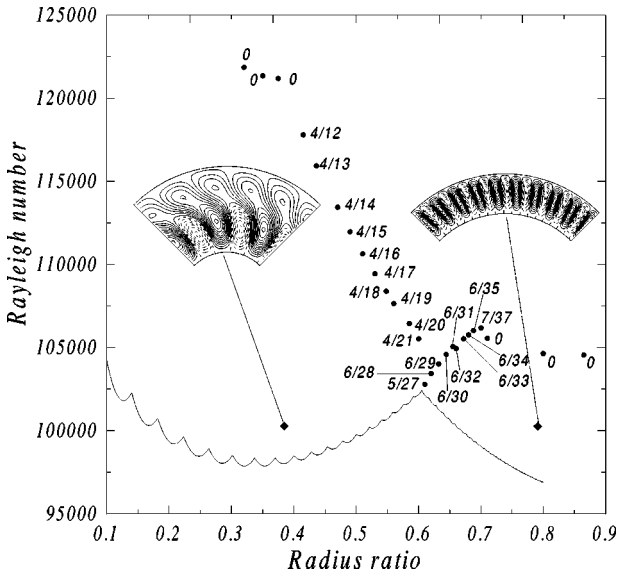

FIG. 1. Critical Rayleigh number as a function of the radius ratio for $\tau=8000$ and $\sigma=0.7$. Solid circles denote the values of the Rayleigh number for which the solution that bifurcates from the marginal curve destabilizes. The numbers near these circles indicate the value of d_m responsible for the instability. The streamlines in the rotating frame of reference of the cylinder of two nonlinear solutions at $\mathrm{Ra}=100\,000$ are also included. These solutions come from the dominant modes $M=10$ (*spiral*) for $\eta=0.35$ and $M=37$ (*normal*) for $\eta=0.7$.

$$\psi'(r,\tilde{\theta})=\psi(r,\tilde{\theta})-\int_{r_i}^{r} f(r)\,dr; \tag{3.1}$$

so, ψ' is zero at the inner surface. Solid lines will denote positive values and dashed lines negative ones. In Fig. 1, the points where the solution that bifurcates from the conductive state at the critical Rayleigh number loses stability are represented by solid circles. The corresponding values of the parameter d_m responsible for every bifurcation are also indicated.

As expected, for $\eta \to 1$ and for a fixed value of τ, we found that the critical Rayleigh number of the *normal* convection $\mathrm{Ra}_c^{(n)}$ tends to the critical Rayleigh number for the small-gap approximation $\mathrm{Ra}_c^{(sg1)}$. In addition, the critical wave number $M_c^{(n)}$ and the corresponding drift rate for $\eta \approx 1$ can be estimated by $M_c^{(n)} \approx \alpha_c^{(sg1)} \overline{r}$ and $\omega_c^{(n)} \approx c_c^{(sg1)}/\overline{r}$, where $\alpha_c^{(sg1)}$ and $c_c^{(sg1)}$ are the critical wave number and the corresponding drift rate for the small-gap approximation, and where $\overline{r} = (1+\eta)/2(1-\eta)$ is the mean radius of the annular shell.

If for $\eta \to 1$ and for a fixed value of τ, the dominant modes among the *spiral* ones are obtained, we observe that the critical Rayleigh number $\mathrm{Ra}_c^{(s)}$ of this type of modes tends to the critical Rayleigh number $\mathrm{Ra}_c^{(sg2)}$ of the κ invariant modes of the problem in the small-gap approximation. Since the potential ψ and the temperature field Θ of these modes are zero at the midplane, they will be referred to as the *second radial harmonics*. The wave number and drift rate of the *spiral* modes for $\eta \approx 1$ can now be estimated by $M_c^{(s)} \approx \alpha_c^{(sg2)} \overline{r}$, and $\omega_c^{(s)} \approx c_c^{(sg2)}/\overline{r}$, where $\alpha_c^{(sg2)}$ and $c_c^{(sg2)}$ are the critical wave number and the corresponding critical drift rate of the *second radial harmonic*. Provided that the values of $\alpha_c^{(sg1)}$ and $\alpha_c^{(sg2)}$ are different, the wave number M of the dominant *normal* mode, and of the dominant *spiral* mode for the same value of η, are different. When η decreases, the critical Rayleigh number for the *spiral* modes decreases and the critical Rayleigh number for the *normal* modes increases, and for a value η_c, the *spiral* modes become the dominant modes. Since usually $\alpha_c^{(sg2)} < \alpha_c^{(sg1)}$, this could explain the forward jump observed between the wave number of the dominant *spiral* mode and that of the dominant *normal* mode at η_c (from $M=21$ to $M=27$ in the case $\tau=8000$, see Fig. 1). A similar tendency was obtained in the small-gap approximation with conical end surfaces [8]. In this paper and subsequent papers, the tangent of the angle of inclination of the lids was expressed by $\gamma = \gamma_0[1+\epsilon f(x)]$, where $\gamma_0 \ll 1$. Despite the different boundary conditions, notice also the resemblance between our solutions depicted in Fig. 1 and solutions of that paper for $\epsilon=1$ and $f(x)=x$ (Fig. 6 of Ref. [8]).

A. Uniform rotating waves

The bifurcation of the conductive state, when perturbations of wave number M are considered, is a Hopf bifurcation in a system with symmetry $\mathbf{SO}(2)$. Then according to Ref. [23], there is a unique branch of periodic solutions consisting of rotating waves with $\mathbf{Z}_M$ spatial symmetry, which bifurcate from this state. Solutions belonging to this branch (primary solutions) or to other branches related in some way to them, are analyzed in this section. These solutions will be connected mainly with those obtained in the small-gap approximation of the problem with $\epsilon=0$ (without curvature), analyzing the effect of breaking the midplane symmetry. For this reason, it is necessary to calculate solutions of this problem, and this has been done using the same numerical techniques as described in the previous section. The corresponding equations can be found in the numerous works of F. H. Busse and collaborators, and are not reproduced here.

In Figs. 2(a), 2(b), and 2(c) we display with solid lines, the Nusselt number $\mathrm{Nu}-1$, the drifting rate ω, and the ratio of energies r_f, of solutions corresponding to rotating waves of $M=17$ for $\eta=0.6$ and $\tau=2800$. The solution that corresponds to the branch bifurcating from the conductive state at $\mathrm{Ra}_c = 25\,439$, comes from the dominant mode of the linear problem at these values of η and τ. This mode is of *normal* type. In order to make clear the above quoted connection of these solutions with those of the small-gap approximation, we have also displayed in Fig. 2(a), with dashed and dotted lines, the Nusselt number of these latter solutions for the same value of τ and wave number $\alpha_c^{(sg1)}=8.68$ corresponding to the critical value for this τ; the critical Rayleigh number is $\mathrm{Ra}_c^{(sg1)} = 24\,624$. Dashed lines represent the *symmetric thermal Rossby waves*, which present a symmetric mean flow profile as a consequence of being $T_{a/2}\kappa$ invariant ($a = 2\pi/\alpha$). The dotted line branch represents solutions that are no longer $T_{a/2}\kappa$ invariant. This branch appears in a secondary bifurcation of the branch of solutions that bifurcate from the conductive state; a pitchfork that breaks the $T_{a/2}\kappa$ symmetry of the primary solutions and gives rise to the so-called *mean flow* solutions in Refs. [9,10]. When the curvature of the annulus is considered, the symmetry κ of the system is broken, and the bifurcation can be seen as the imperfect bifurcation observed in Fig. 2(a), with the corresponding splitting of the dotted line branch in branches 1 and 2. This feature was anticipated in Ref. [10], although in that work, by also considering a small-gap approximation, the symmetry κ was broken including the effect of conical ends. The disconnected curve of the solutions of the problem in the small-gap approximation (again $T_{a/2}\kappa$ invariant solutions) is one of the curves of the imperfect bifurcation that comes from a pitchfork bifurcation in the $\tau=0$ problem (equivalent to Rayleigh-Bénard). This is the steady bifurcation of a roll state that, breaking the reflection symmetry R (absent in the $\tau \neq 0$ case)

$$R: \quad (x,y) \to (x,-y), \quad (f,\psi,\Theta) \to (-f,-\psi,\Theta),$$

maintains the shift-reflect symmetry. This bifurcation produces states that drift either in one direction or the other with the same drift rate [24,25], and related between one to the other by the reflection R, for suitable chosen origins in y. The drift speed, which vanishes at the bifurcation point, increases away from it as the square root of the distance from the bifurcation point. When the Coriolis term is included, the symmetry R is broken and an imperfect bifurcation is formed.

With respect to the stability of the $\eta=0.6$ branches, the branch labeled 1 is stable from the bifurcation of the conductive state to $\mathrm{Ra}=32\,540$; the branch labeled 2 is stable from

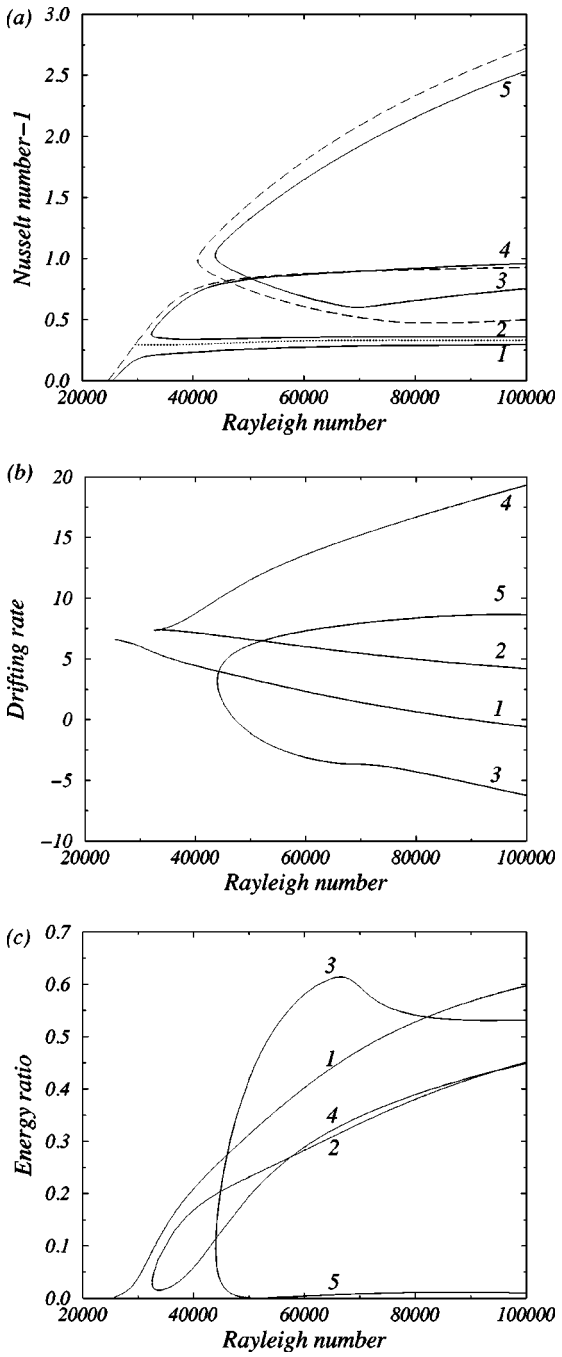

FIG. 2. (a) Nusselt number Nu−1, (b) drift rate ω, and (c) ratio of energy associated to the mean flow r_f, versus the Rayleigh number Ra of uniform drifting waves. Solid lines correspond to solutions of wave number $M=17$ at a radius ratio $\eta=0.6$. In (a) dashed lines (*shift-reflect* invariant solutions) and the dotted line correspond to solutions for the problem in the small-gap approximation ($\alpha_c^{sg}=8.68$). In both cases, the solutions that bifurcate from the conductive state come from the the dominant modes of the linear stability analysis of this state; $\tau=2800$ and $\sigma=0.7$.

the saddle point at Ra=32 532 to Ra=33 785. Two different stable solutions with the same wave number then coexist for a small range of values of the Rayleigh number. In both cases the bifurcation is superharmonic ($d=0$). The rest of the branches are unstable. Figure 2(b) shows how the drift of the solutions corresponding to branches labeled 1, 2, and 3 tends to decrease when the Rayleigh number increases, with an opposite tendency for the solutions in branches 4 and 5. This figure also shows that for the highest values of the Rayleigh number considered, the solutions in branches 1 and 3 drift in the retrograde direction. In Fig. 2(c) we can appreciate the small contribution of the zonal flow to the total stream field for solutions in branch 5, and how for the solutions in the rest of the branches this contribution is about 50% for sufficiently high Rayleigh numbers in the range considered. Since the kinetic energy of the fluctuating component of motion $\langle E_k' \rangle$ exhibits a similar behavior to the Nusselt number when the Rayleigh number varies (although the rate of change is different depending on the type of solutions), the decrease in the Nusselt number for branch 3 is accompanied by a notable increase of the value of r_f [see Figs. 2(a) and 2(c)]. The effect is similar, although not so sharp, when the Nusselt number remains practically constant, as occurs in branches 1, 2, and 4.

In Figs. 3(a) and 3(b), we show at a fixed instant the streamlines and the contour plots of the temperature field Θ in the rotating frame of reference of the cylinder, corresponding to different solutions at Ra=60 000. Starting from the top in a counterclockwise direction, they belong to the branches labeled 1, 2, 3, 4, and 5 in Fig. 2. To plot this figure, we have maintained the number of different contour levels. Therefore, the interval between contour levels for the different solutions is not the same. Solutions corresponding to branches 1 and 2 are those coming from the splitting of the mean flow solutions, and as discussed in Ref. [9], they are characterized by a small Nusselt number due to the shift of the convection eddies. For the solutions in branch 1, however, this shift is towards the outer surface of the shell and the velocity field is cyclonic relative to the rotating system. For the solutions in branch 2, the shift is towards the inner surface and the velocity field is anticyclonic. Figure 3(c) shows the corresponding cyclonic and anticyclonic shear for the solutions in branches 1 and 2, respectively. The solutions in branches 3 and 4 present a strong zonal flow in the middle of the shell, retrograde for solutions in branch 3 and prograde for solutions in branch 4. The convection eddies are shifted to the inner and outer parts of the shell, anticyclonic (cyclonic) in the inner part and cyclonic (anticyclonic) in the outer part for the solutions in branch 3 (4). The solutions in branch 5 look like rotating Taylor columns with a small zonal flow, prograde in the middle of the shell. Since convection occupies all the layer, the Nusselt number for this solution is the biggest one. This last type of solution was also obtained by Ref. [11].

In Figs. 4(a), 4(b), and 4(c) we represent with solid lines, the Nusselt number Nu−1, the drifting rate ω, and the ratio of energies r_f, of uniform rotating waves of wave number $M=21$ for $\eta=0.6$ and $\tau=8000$. The primary solution, which bifurcates at $\mathrm{Ra}_c=102\,156$, comes from the dominant mode for these values of η and τ. Now it is a *spiral* mode. For these values of the parameters, only solutions in branch 1 are stable, but within a small region of the Rayleigh number values. They lose stability at Ra=105 517 via a subharmonic instability. At this point, the solutions still maintain their

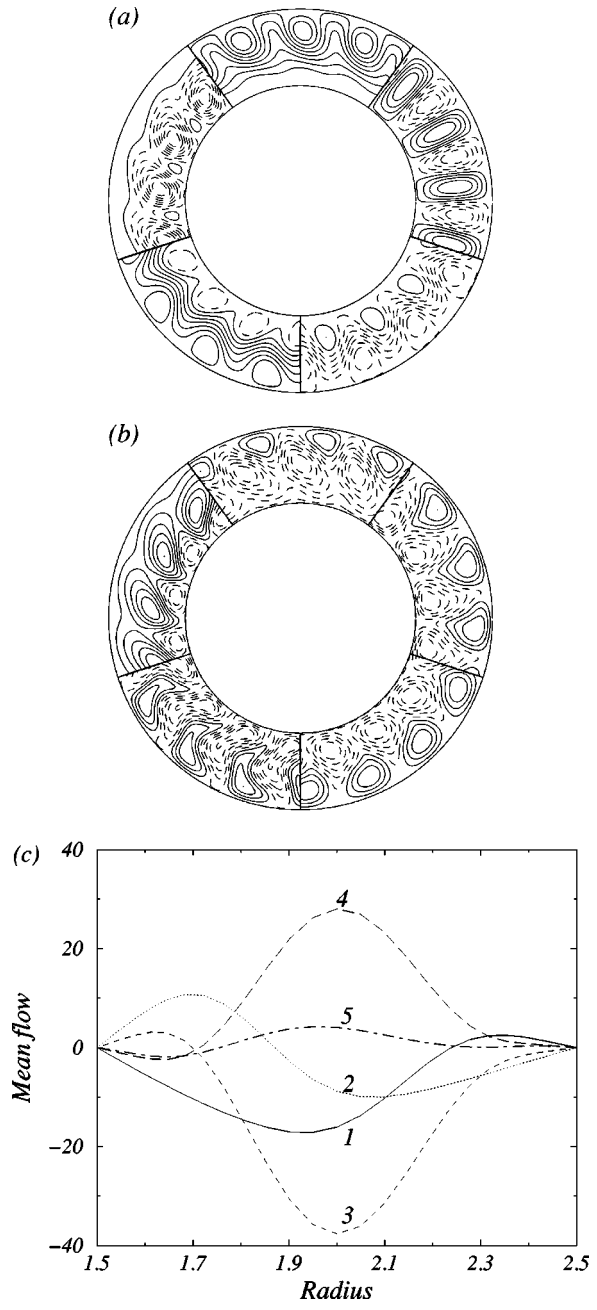

FIG. 3. Temperature field Θ, at a fixed instant in the rotating frame of reference of the cylinder, of the solutions corresponding to the branches 1, 2, 3, 4, and 5 in Fig. 2 for Ra=60 000. (c) The zonal mean flow of the same solutions; η=0.6, $M=17$, τ=2800, and σ=0.7.

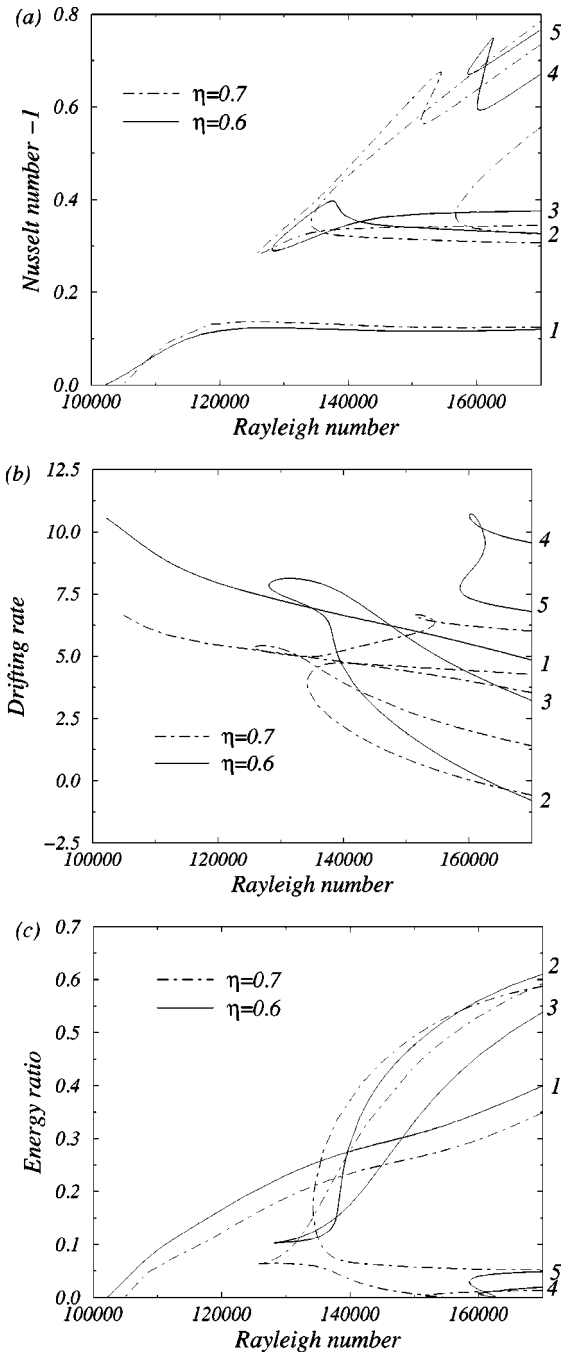

FIG. 4. (a) Nusselt number Nu−1, (b) drift rate ω, and (c) ratio of energy associated to mean flow r_f, versus the Rayleigh number Ra, for uniform drifting waves of wave number $M=21$ and η=0.6 (solid lines) and of $M=32$ and η=0.7 (dotted-dashed lines). The solution that bifurcates from the conductive state for η=0.6 comes from the dominant mode (*spiral*) for these parameters. The solution that bifurcates from the conductive state for η=0.7 comes from the dominant mode among the *spiral* ones for these parameters; τ=8000 and σ=0.7.

spiral character (similar to the solution in Fig. 1) with a small cyclonic shear. As we will see later, for this value of the Coriolis parameter, the stability zone of the primary solutions for aspect ratios near the η_c, the crossing of dominant families of modes, is notably reduced. As in the previous case, solutions in branches that do not present an increase of the Nusselt number when the Rayleigh number increases, are the ones that show a faster growth rate of the contribution of the kinetic energy of the zonal flow to the total kinetic energy.

Unlike the previous case, this scenario of branches and the connection between them transforms when $\eta\rightarrow 1$. In the same figure we have also depicted with dotted-dashed lines, branches of solutions of wave number $M=32$ for η=0.7, where the solution that bifurcates from the conductive state

no longer arises from the dominant mode (for these values of η and τ, it is a *normal* one) but comes from the dominant mode among the *spiral* ones. In Figs. 4(a), 4(b), and 4(c), we can observe how for $\eta=0.6$ the two disconnected curves are formed by branches 2-3 and 4-5, whereas for $\eta=0.7$ they are formed by their counterparts 3-4 and 2-5. In addition, for this last value of η, a new disconnected curve appears in the range of the values of the Rayleigh number considered in the figure, and moves towards higher values of the Rayleigh number for $\eta=0.6$.

Figures 5(a) and 5(b) show in a fixed instant and in the rotating frame of reference of the cylinder, the streamlines and the contour plots of the temperature field of the different solutions obtained for Rayleigh number $\mathrm{Ra}=170\,000$, $\eta=0.6$, and $\tau=8000$. Starting from the top, in a counterclockwise direction, they correspond to solutions in branches 1, 2, 3, 4, and 5 of Fig. 4. The solution corresponding to branch 1 is characterized by a retrograde mean flow in the inner part, greater than the prograde mean flow in the outer part [see Fig. 5(c)]; the shear is sufficient to shift the spiral structure to the outer part of the shell. The solutions corresponding to branch 2 exhibit a retrograde mean flow that is maximum in the middle of the shell, and present anticyclonic convective eddies in the inner part of the shell; the fluid in the outer part of the annulus remains practically stagnant in the rotating frame of reference of the cylinder. Solutions in branch 3 present a retrograde zonal mean flow in the middle part of the shell, and the convective eddies are shifted to the inner and outer parts of the shell, anticyclonic in the inner part and cyclonic in the outer part. The spiral effect of solutions corresponding to branches 4 and 5 is very small. They present a shear that is not sufficient to destroy the double roll columnar structure, and they look like two stacked rotating *normal* columns. Notice how the solution corresponding to branch 3 resembles the solution depicted in Fig. 3, which belongs to the branch 3 of Fig. 2. In fact for $\tau=8000$, $\eta=0.9$, and $M=122$, the counterpart branch of branch 3 of Fig. 2 connects with the counterpart of branch 3 of Fig. 4, via a saddle-node bifurcation.

In order to match the branches of solutions obtained in Fig. 4 with those of the small-gap approximation, in Fig. 6(a) [Figs. 6(b) and 6(c) are enlargements of two zones in Fig. 6(a)] we plot with dashed and dotted lines the Nusselt number $\mathrm{Nu}-1$, as a function of the Rayleigh number of the solutions corresponding or related to the dominant *second radial harmonic* of the problem with this approximation. The critical α of this harmonic for $\tau=8000$ is $\alpha_c^{(sg2)}=11.37$, and the critical Rayleigh number is $\mathrm{Ra}_c^{(sg2)}=106\,330$. Dashed lines now represent solutions that are κ invariant (also with midplane symmetric mean flow profile), and dotted lines represent branches of solutions without any symmetry, except those associated to spatial and time periodicity. The dotted-line branches, e and d, appear as a consequence of two pitchfork bifurcations that break the symmetry κ of branches a and b, respectively. These bifurcations are indicated by a small square in the Figs. 6(a) and 6(b). The dotted-line curve formed by branches f–g is a disconnected one (it has been checked up to values of the Rayleigh number near $\mathrm{Ra}=300\,000$). These dotted-line branches of solutions split

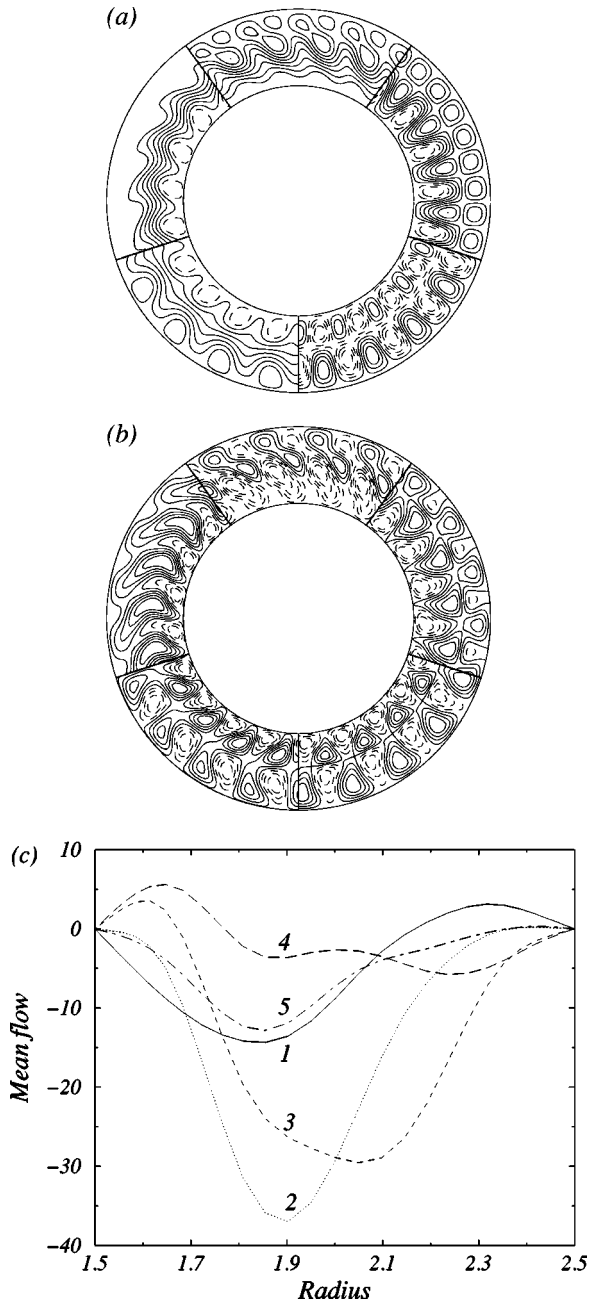

FIG. 5. From the top, in a counterclockwise direction, (a) streamlines, (b) contour plots of the temperature field Θ, at a fixed instant in the rotating frame of reference of the cylinder, of solutions corresponding to the branches 1, 2, 3, 4, and 5 in Fig. 4 for $\mathrm{Ra}=170\,000$. (c) The zonal mean flow of the same solutions; $\eta=0.6$, $M=21$, $\tau=8000$, and $\sigma=0.7$.

when the symmetry κ is broken. The dashed curve a–b is again the disconnected curve of the imperfect bifurcation that arises from a pitchfork bifurcation in the $\tau=0$ problem, when the reflection symmetry R is broken due to the Coriolis term. This pitchfork is the steady bifurcation of two stacked rolls that breaks the symmetry R but maintains the κ symmetry. In Figs. 6(a), 6(b), and 6(c), the Nusselt number of solutions for $\eta=0.9$ and wave number $M=108$ is also plotted (solid lines). The solution that bifurcates from the con-

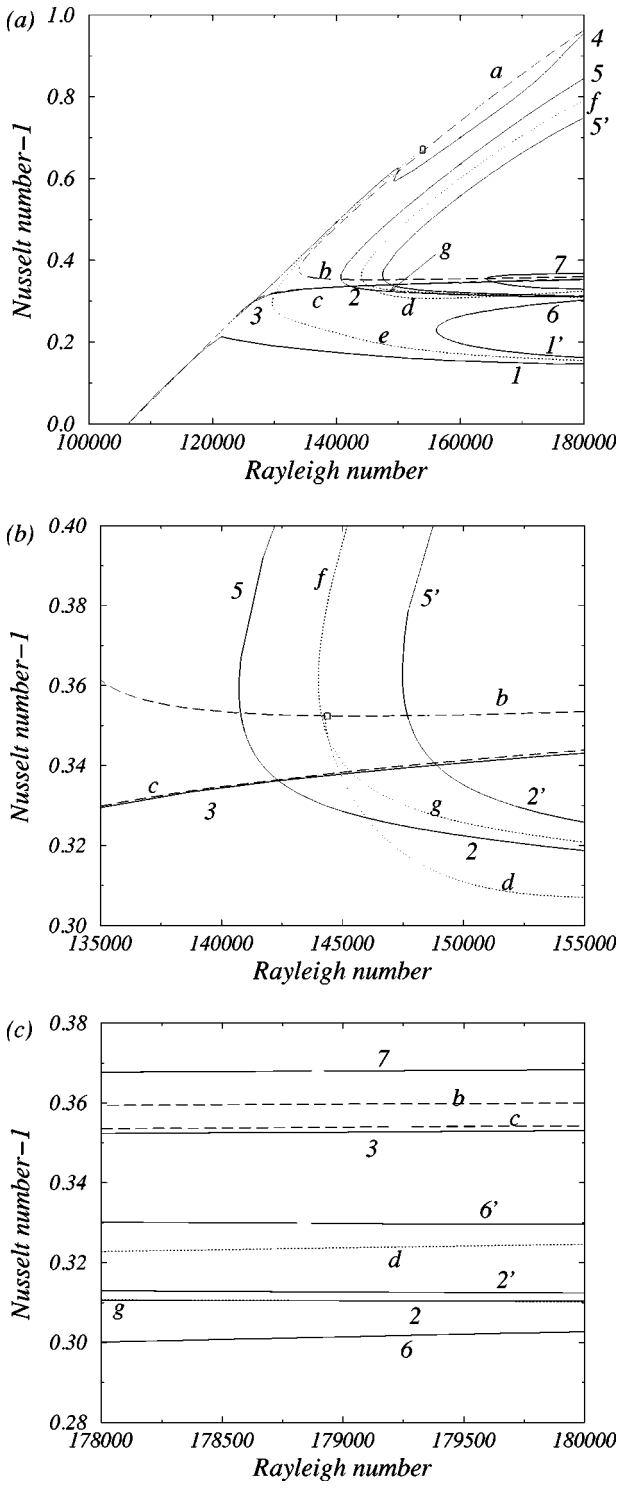

FIG. 6. (a) Nusselt number of uniform rotating waves versus the Rayleigh number Ra. Solid lines correspond to solutions of wave number $M=108$ for a radius ratio $\eta=0.9$. Dashed lines (κ invariant solutions) and dotted lines correspond to solutions for the problem in the small-gap approximation ($\alpha_c^{(sg2)}=11.37$). In both cases, the solutions that bifurcate from the conductive state have the wave numbers that correspond to the preferred modes among the *spiral* modes for $\eta=0.9$ and among the *second radial harmonic* for the small-gap approximation. (b) and (c) are enlargements of some zones in (a); $\tau=8000$ and $\sigma=0.7$.

ductive state is obtained from the dominant mode among the *spiral* ones. The labels of the branches in these figures are chosen to identify the branches of solutions obtained for $\eta=0.6$ (see Fig. 4). The correspondence between branches for the small-gap approximation and for $\eta=0.9$ can easily be done if the values of the Nusselt number, frequencies, ratio of energies, and patterns (not shown here) are compared for the higher values of the Rayleigh numbers of the figure. This correspondence is the following: dashed branches a, b, and c become branches 4, 7, and 3, respectively; and branches d, f, g, and e split in branches 6-6', 5-5', 2-2', and 1-1', respectively. However, the transition of the picture of branches for the small-gap approximation to that obtained for $\eta=0.9$ is not so clear in the intermediate range of values of the Rayleigh number analyzed.

In Fig. 7 we display for different values of τ, the Nusselt number $\mathrm{Nu}-1$, the drift rate ω, and the ratio of kinetic energies r_f, as a function of the control parameter $\delta=(\mathrm{Ra}-\mathrm{Ra}_c)/\mathrm{Ra}_c$ corresponding to the nonlinear solutions that result from the preferred mode bifurcating from the conductive state. Solutions in annulus of radius ratios $\eta=0.6$ and $\eta=0.5$ are considered. The dominant modes for $\tau=2800$ and 4000, are *normal*, and for $\tau=8000$ and 11 000 they are *spiral*. In the description of these results, we refer to solutions that come from *normal* modes and *spiral* modes as normal solutions and spiral solutions, respectively, although for not very small values of δ, we already know that the *normal* and *spiral* character is not mantained. For the chosen values of τ, the branches of normal and spiral solutions present a similar behavior to branches 1 in Figs. 2 and 4, respectively. The sudden change in the slope of the Nusselt and r_f for the solution of $\tau=11\,000$, also appears in that of $\tau=8000$ for higher values of δ, although with less slope. Our results show that, for solutions of the same family, the efficiency in transporting heat decreases when τ increases. This effect, according to Ref. [13], could be due to the increase of the drifting [see Fig. 7(b)], which hinders the fluid parcels from travelling from the hot to the cold boundary. The slopes for small values of δ also depend on the value of τ. This differs from the results of Ref. [8] for the small-gap approximation and stress-free boundary conditions, where the Nusselt number is at lowest order independent of the Coriolis parameter τ. When the radius ratio η decreases, we observe a decrease in the values of the Nusselt number for the same values of τ and δ, provided that the solutions are of the same type. Once again, this can be explained by the increase of the corresponding drift. For small values of δ, we have also compared the efficiency in transporting heat of solutions coming from the dominant *normal* mode and the dominant *spiral* mode for the same values of τ and η, and we have found that the one associated to the *spiral* mode is more efficient.

Since the degree of spiraling of the *spiral* modes is much higher than that of the *normal* ones [12], their nonlinear interactions will produce larger Reynolds stresses, resulting in a bigger mean flow [4]. Thus, the growth rate of r_f for the spiral solutions at small values of δ exceeds those of the normal solutions. Moreover, the spiral solution at small values of δ exhibits a growth of the ratio of kinetic energies r_f, with increasing δ stronger than the part of the normal solu-

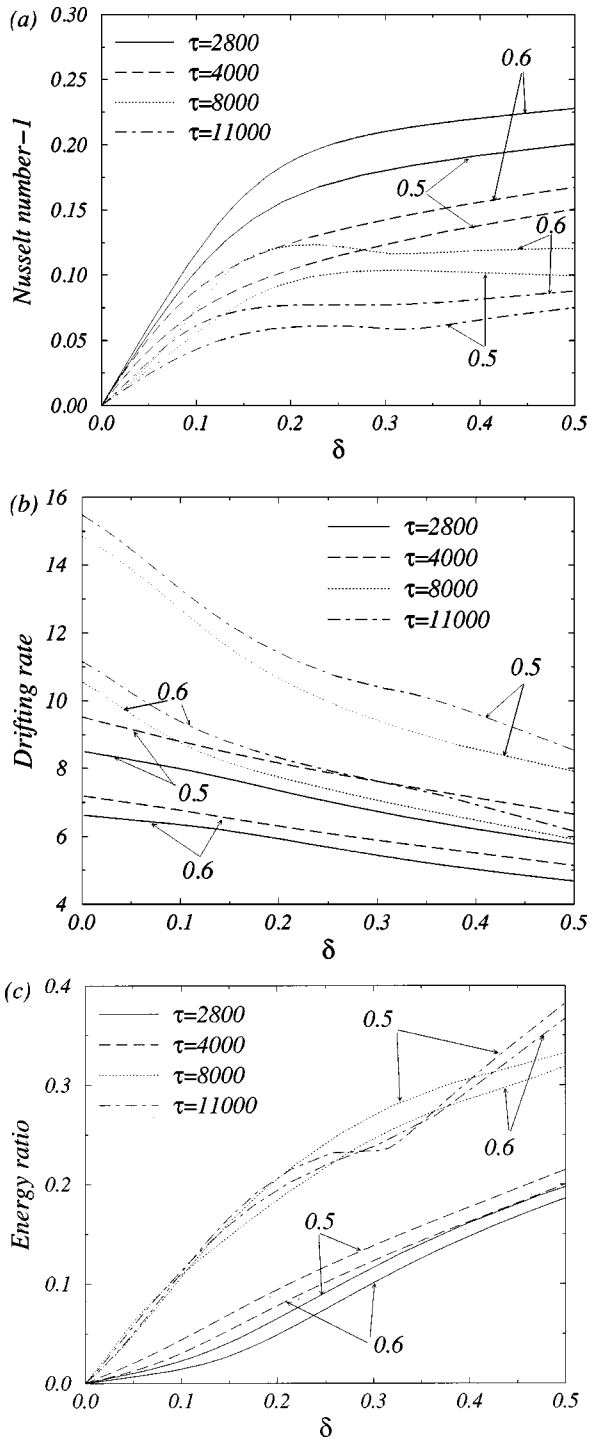

FIG. 7. (a) Nusselt number $\mathrm{Nu}-1$, (b) drift rate ω, and (c) ratio of energy associated to mean flow r_f, versus the parameter $\delta=(\mathrm{Ra}-\mathrm{Ra}_c)/\mathrm{Ra}_c$ of the solutions that bifurcate from the conductive state for $\eta=0.6$ and $\eta=0.5$ for different values of τ. These solutions come from the dominant modes of the linear stability of the conductive state, *normal* for $\tau=2800$ and 4000, and *spiral* for $\tau=8000$ and 11 000; $\sigma=0.7$.

tions that comes from the ''mean flow solution.'' When η decreases from $\eta=0.6$ to $\eta=0.5$, the degree of spiraling of the dominant modes for the same value of τ is observed to increase. This explains our results in Fig. 7(c) for the normal solutions at small values of δ. However, for the spiral solutions, the slope of r_f and the averaged kinetic energy associated to the mean flow at small values of δ, decreases when η does. This suggests that other factors, in addition to the degree of spiraling, must be taken into account if this behavior is to be understood. As we commented above, the kinetic energy of the fluctuating part shows a dependence on the Rayleigh number similar to the Nusselt number. However, the scaling depends on the solution. For example, although the Nusselt number of the normal solution for $\tau=2800$ is bigger than the spiral one for $\tau=8000$, the kinetic energy $\langle E_k' \rangle$ associated to the normal solution for $\tau=2800$ is smaller than that of the spiral one for $\tau=8000$.

B. Instabilities of the primary solutions

In this section, we analyze the stability of the uniform rotating waves presented previously. We mainly consider the solutions corresponding to the branches that bifurcate from the conductive state and which come from a dominant mode in some region of the space of parameters. As we commented above, in Fig. 1, we indicate by solid circles the values of the Rayleigh number where the primary solutions, for $\tau=8000$ and for different values of η, destabilize. All these solutions arise from the preferred modes for the chosen values of η. The figure shows how the stability region of the solutions reduces considerably near the transition point, $\eta_c=0.605$, corresponding to the crossing of the two different families of dominant modes. Near this point, the primary solutions destabilize with a finite value of the parameter d_m, irrespective of whether they come from a *spiral* or from a *normal* mode. For both smaller and higher values of η far from η_c, we obtain a zone where the selected primary solutions lose stability by means of a superharmonic instability ($d_m=0$). For values of η very near 1, the value of d_m is finite but relatively small, agreeing with our results for the small-gap approximation for this value of τ and wave number corresponding to the critical value $\alpha_c=12.8$. In this approximation, we find that the mean flow solution destabilizes with a value of $d\approx 0.007$, where the wave numbers excited by using an expression similar to Eqs. (4a) and (4b), are $(n+d)\alpha$. As discussed in Sec. II, from the values of the parameter d_m (also indicated in the figure) responsible for the bifurcation, the wave numbers excited are known, and the corresponding eigenfunction at the bifurcation point can be examined in order to check which wave number of the perturbation has associated the maximum amplitude [see Eqs. (4a) and (4b)], and what the corresponding pattern is like. For the solutions that arise from the dominant modes near η_c (finite d_m), we obtain that for those coming from the *spiral* modes (on the left of η_c), the maximum coefficients (b_{nj}^*, c_{nj}^*) of the eigenfunction correspond to the index $n=1$, so the perturbation is dominated by a periodic structure of wave number $M+m$, with M being the wave number of the primary solution. We have also ascertained that the associated pattern is of *normal* type. For the solutions that come from the columnar modes (on the right of η_c), the maximum coefficients correspond to the index $n=-1$, so the dominant wave number in the perturbation is $M-m$, and in this case

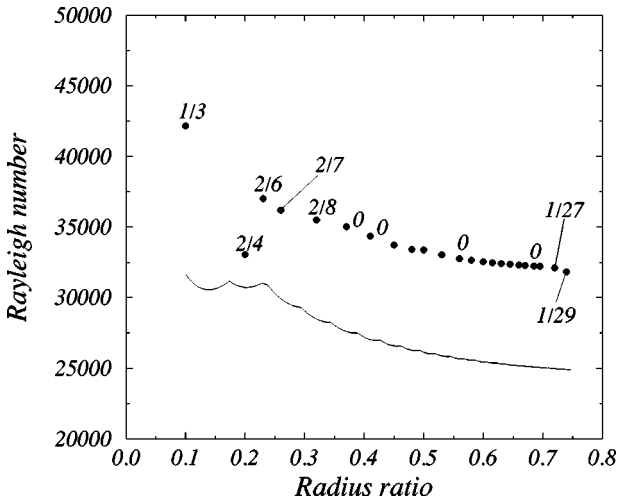

FIG. 8. Critical Rayleigh number as a function of the radius ratio for $\tau=2800$ and $\sigma=0.7$. Solid circles denote the values of the Rayleigh number for which the solution that bifurcates from the marginal curve destabilizes. The numbers near these circles indicate the value of d_m responsible for the instability.

the associated pattern is of *spiral* type. Thus, it can be summarized that in this region (near the crossing of different type of dominant modes), for a fixed value of η, a nonlinear solution coming from a dominant mode of one type, *spiral* or *normal*, is destabilized by a perturbation of the other type of mode (*normal* or *spiral*, respectively). We have also checked that for this value of the Coriolis parameter, $\tau=8000$, the wave number of the perturbation having the maximum amplitude always corresponds to one of the other type of modes that has already bifurcated from the conductive state for the same value of η [see Fig. 5(a) in Ref. [12]].

In Fig. 8, we present the results for the case of $\tau=2800$. The marginal curve of the conductive state is represented by a solid line, and in this case the crossing of the different dominant modes takes place at $\eta_c=0.228$. The wave number of the preferred mode (*spiral*) before the transition is $M=4$, and that of the preferred one (*normal*) after the transition is $M=6$. Again, near the transition point, the nonlinear solutions coming from the preferred modes destabilize with a finite value of d_m. Examination of the eigenfunction corresponding to the eigenvalue responsible for the bifurcation shows that the solutions coming from one type of mode are destabilized by a perturbation dominated by the other type. When η increases, we obtain a large zone where the bifurcation is superharmonic ($d_m=0$); and similar to that obtained for $\tau=8000$, when η is near one, the solution destabilizes again with a finite and small value of d_m, agreeing with the results of Ref. [10] for the destabilization of the mean flow solution for this value of τ and wave number $\alpha_c=8.68$.

In a previous paper [26], we analyzed some secondary solutions near the secondary bifurcation. The results were obtained by using a nonlinear time dependent code, similar to the one in Ref. [17], which integrates the Navier-Stokes equations in primitive variables by employing a second-order stiffly stable splitting method. One of the cases studied was the solution that bifurcates from the uniform drifting wave of wave number $M=21$, which comes from the dominant *spiral* mode for $\eta=0.6$ and $\tau=8000$ (see Fig. 1). The value of d_m, responsible for the bifurcation, is in this case 4/21, and as we have commented above, the wave number of the perturbation having the maximum amplitude is $M=25$. We observed that the secondary solution presented a set of 25 pairs of rolls in the outer part of the layer and a set of 21 in the inner part, each set being propagated at its own speed. Thus, the secondary solution has a dynamic similar to the double-column convection obtained by Ref. [10] for the problem in the small-gap approximation with conical ends. Another case considered was the secondary solution that bifurcates from the uniform rotating wave of wave number $M=17$ coming from the dominant *normal* mode for $\eta=0.6$ and $\tau=2800$ (see Fig. 8). The convection in the primary solutions, just before the bifurcation, was confined in the outer part of the layer. The secondary solution, appearing from a superharmonic bifurcation ($d_m=0$) oscillated between this structure and one in which convection was restored in the whole of the layer. This feature resulted in a notable increase of the heat transport. The effect of the instability is then similar to the vacillating instability described in Ref. [9,10].

As well as considering the instabilities of the primary solutions when the Rayleigh number is increased from its critical value, we have also analyzed for a fixed value of the Coriolis parameter τ, the stability zone of the M-rotating waves coming from the dominant modes for some value of η when, fixing the value of M, the value of the radius ratio varies beyond the range where the corresponding M mode is dominant (sideband stability). In a radius ratio Rayleigh number diagram, the side stability zone of a M-primary solution is always bounded by curves arising at the crossing points between the critical curve of the M mode, and the curves of the two adjacent dominant modes M_l and M_r, when η is decreased and increased, respectively. If, near a crossing, we calculate from the values of d_m responsible for the sideband instabilities the wave numbers excited, and from the corresponding eigenfunction we check which one has maximum amplitude, the wave number of the adjacent mode at the crossing is always obtained. Moreover, when we estimate from the imaginary part of the eigenvalue the frequency of this harmonic, we obtain that of the adjacent mode at the primary bifurcation. Thus, as expected, the interaction of the neighbor modes, nonresonant in all the cases studied, is responsible for the sideband instability. However, the shape of these side stability boundaries depends on whether the value of η is near the crossing of the two types of different dominant modes η_c.

If the primary solution considered comes from a dominant mode for η far from η_c, the side boundaries have a parabolic shape, irrespectively of whether the dominant mode is *normal* or *spiral*. See, for example, in Fig. 9 the stability limits (solid circles) of the primary solutions of wave number $M=20$ for a Coriolis parameter $\tau=2000$. When η varies, the wave numbers of the dominant modes of the same family are sequential ($M_l=M-1$, $M_r=M+1$). Then the value of d_m of the preferred sideband disturbance, near the value of the intersection of the adjacent modes, is $d_m=1/M$ on both

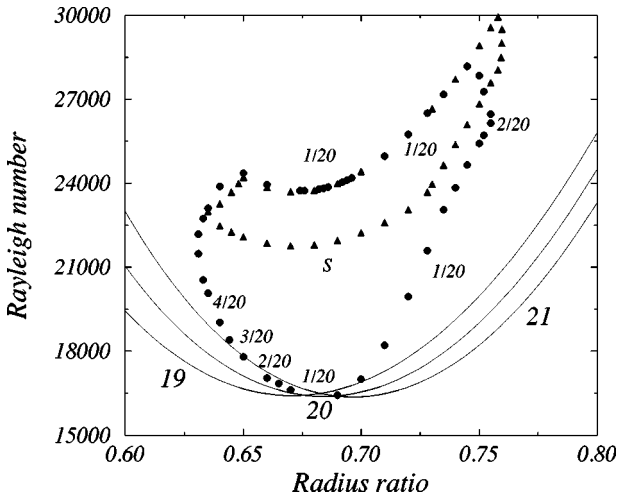

FIG. 9. Stability boundaries of rotating waves with wave number $M=20$. Solid circles for solutions in the branch that bifurcates from the critical curve for this wave number, and solid triangles for the solutions in the lower branch of the disconnected curve similar to the one in Fig. 2. The values of d_m responsible for these limits are given at the stability boundaries. *S* means that the stability limit corresponds to the saddle-node point of the disconnected curve. The values *M* of the critical curves are also indicated; $\tau=2000$ and $\sigma=0.7$.

sides. So, far from η_c, for the values of η corresponding to the crossings of the preferred modes, there exist zones (*V*-shaped in the diagram $\eta-\mathrm{Ra}$) where at least two uniform drifting states with sequential wave numbers are stable. When the Rayleigh number is increased from the values at the crossings, we obtain for the solutions coming from the *normal* modes (see Fig. 9), that on the left-side boundary d_m increases (m increases sequentially) in such a way that the disturbance is dominated by the coefficients associated to the wave numbers of the dominant modes for the values of η that are reached by this boundary, or for even smaller values. However, the right-side stability boundary corresponds to a value of $d_m=1/M$, and the disturbance is dominated by the wave number $M+1$. In fact, for the solutions coming from the *normal* modes, if from the values of *M* and η, we estimate the value of the equivalent wave number α of the solutions in the small-gap approximation, we retrieve the results corresponding to the sideband instabilities of the symmetric thermal Rossby waves discussed in Ref. [9,27,10,28,29]. For a value of the Prandtl number $\sigma=0.7$, the referred works found that the left sideband instability in a diagram (α, Rayleigh number) corresponds to infinitesimal values of the Floquet parameter and has the tendency to increase the value of α slightly, shifting the solution towards the stable zone, but very close to the left-side stability boundary. On the other hand, the right sideband instability, associated to finite values of the Floquet parameter, tended to shift the unstable solution towards one with a value of α smaller than α_c but near it. Notice that for a fixed value of *M*, increasing η has the effect of decreasing α, and that for a fixed value of η, increasing *M* has the effect of increasing α.

In Fig. 9 we also indicated by solid triangles the limits of the stability zone of the solutions that belong to a branch, equivalent to branch 2 of Fig. 2. Thus, in the intersection of the stability zones limited by solid circles and solid triangles, two different stable drifting waves with the same wave number exist. For values of $\eta<0.72$, the patterns of the rotating waves of wave number $M=20$ that belong to the branch that bifurcates from the conductive state and those of the lower branch of the disconnected curve are similar to their counterparts in Fig. 3 ($\tau=2800, \eta=0.6$), i.e., the solutions bifurcating from the conductive state turn into a solution with the convection eddies shifted to the outer part of the layer when the Rayleigh number increases; whereas for the other solutions this shifting is to the inner part. However, for a value of η between 0.72 and 0.728, a nongeneric pitchfork bifurcation occurs, and for values of $\eta>0.728$, the solutions bifurcating from the conductive state now turn into a solution with the convection eddies shifted to the inner part of the layer when the Rayleigh number increases, and for the other solutions this shifting is to the outer part.

The shape of the side stability boundaries of an *M*-rotating wave, which comes from a preferred mode for a value of η near η_c, is no longer parabolic. In Figs. 10(a) and 10(b), we present for the values of the Coriolis parameter $\tau=8000$ and $\tau=2800$, respectively, the stability limits of the primary solutions arising from both the dominant *spiral* mode (solid circles) and from the *normal* mode (solid triangles), which dominate for the values of the radius ratio η, just before and just after η_c. Thus, for $\tau=8000$, the stability zones correspond to drifting states of wave numbers $M=21$ (*spiral*) and $M=27$ (*normal*), and for $\tau=2800$, they correspond to $M=4$ (*spiral*) and $M=6$ (*normal*) rotating waves. The values of d_m responsible for the stability boundaries are included. In these figures we have also represented, with dashed and solid lines, some of the critical curves of the *spiral* and *normal* modes, respectively, whose interactions control the sideband stability of the selected primary solutions. The values of the wave numbers of these modes are also included.

For $\tau=8000$, the left branch of the stability limit for the solution coming from the *spiral* mode ($M=21$) is parabolic, whereas the right-side branch becomes practically independent of the Rayleigh number. For the solution that comes from the *normal* mode ($M=27$) we observe a shift of the stable region rightward, since the left-side branch has moved to the right. The interaction between the *normal* $M=27$ mode and the *spiral* $M=21$ and 22 modes seems to be responsible for this behavior, as can be deduced from the values of d_m at this branch. Notice that there does not exist any range of parameters for which both the $M=21$ and the $M=27$ rotating waves are stable.

The shape of the stability zones for the solutions coming from the two type of modes near the transition point for the Coriolis parameter $\tau=2800$ is completely different. In this case, the stability zone of the solution that comes from the *spiral* mode is shifted leftward. The interaction between the *spiral* $M=4$ mode and the *normal* $M=6$ mode causes the right-hand stability branch for the $M=4$ drifting wave to move to the left ($d_m=2/4$). With respect to the stability of the solution of wave number $M=6$, the left-side branch has

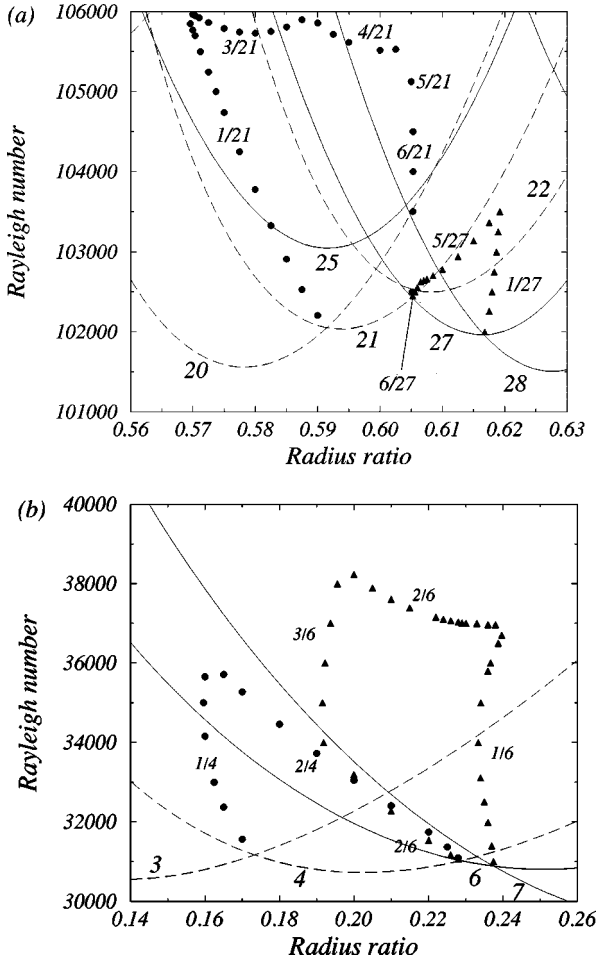

FIG. 10. Stability boundaries of the rotating waves with the wave numbers corresponding to the preferred modes for values of η just before (*spiral*) and just after (*normal*) η_c, for (a) $\tau=8000$ and (b) $\tau=2800$. The stability limits of the solution before (after) η_c are represented by solid circles (triangles). The values of d_m responsible for these limits are given on the stability boundaries. The critical curves of some azimuthal modes (the value of M is indicated) are depicted by dashed (*spiral*) and by solid (*normal*) lines; $\sigma=0.7$.

a parabolic shape, and the values of d_m reveal that the interactions between the $M=6$ *normal* mode and the $M=4$ and $M=3$ *spiral* modes govern this stability boundary. The right-hand side boundary has an almost vertical concave form. The intersection of the stability regions of the $M=4$ and $M=6$ drifting waves is now a thin stripe region leaning to the left of η_c.

IV. CONCLUSIONS

In this paper we analyze nonlinear solutions related to the two types of dominant modes, *normal* and *spiral*, identified in our previous paper [12]. Particular effort is made to connect the solutions in the annulus with those obtained in the small-gap approximation, in order to find out to what extent this approximation can be used. Our nonlinear results show that the small-gap approximation might serve to predict the dynamics in the curved annulus, whenever the dominant mode in the annulus was of *normal* columnar type, and the value of the radius ratio was far enough from the value of η_c for the Coriolis parameter considered. Nevertheless, the effects of the breaking of symmetry κ must be taken into account to describe the scenario of branches and the features of the solutions associated with the *normal* columar modes. When the dominant mode is *spiral*, we show that in this case the connection should be carried out with the solutions related to the dominant κ invariant mode (*second radial harmonic*) in this approximation. However, we find that for these solutions, the scenario of branches transforms significantly when the curvature is included and the value of η starts to decrease from the assymptotic value of one.

The global properties of the primary solutions corresponding to the dominant *normal* and *spiral* modes for different values of the Coriolis parameter and radius ratio, are described at the end of Sec. III A. For the value of Prandtl number considered in this paper, the effects of rotation usually lead to a decrease in the heat transport by convection at the onset, which agrees with the results obtained by Ref. [13] in spherical shells for fluids of Prandtl number $\sigma=1$. Since these primary solutions correspond to different values of the Coriolis parameter and have different wave numbers, it is interesting to analyze the global properties, considering only the influence of the type of mode they arise from. To do this, we calculated the rotating waves, which came from two modes, one of each family, with the same wave number for the same values of τ and η, and we found that for small values of δ, the solutions that stemmed from the *spiral* modes were more efficient in transporting convective heat, had associated a smaller drift, and the contribution of the axysmmetric flow to the velocity field was bigger. Since the Coriolis parameter, radius ratio, and wave number for these solutions were the same, the better correlation between the radial velocity and the temperature field shown by the *spiral* modes, could account for the greater efficiency in transporting heat.

Our paper is not restricted to a calculation of the primary solutions coming from preferred modes. Other rotating waves with the same wave number as the primary solutions are obtained and their nonlinear properties described. Although most of them are unstable, the more information we have about these solutions to the problem, the easier it is to explain the more complex behavior that the solutions of the system may exhibit after the secondary bifurcations. On one hand, we find solutions characterized by a weak mean flow, a remarkable heat transfer, and with a simple or double nondistortioned structure of columns, and on the other hand, solutions with a component of the mean flow containing more than 50% of the total kinetic energy, even for values of the Rayleigh number lesser than two times the critical value [see Fig. 4(c)]. Notice how the effect of the rigid lids is not enough to supress the strong zonal flows of some of the rotating waves. However, we suppose that, for very small supercritical values of the Rayleigh number, the nonslip boundary conditions of our model prevent us from obtaining solutions with mean flows as strong as those in the work of Ref. [4] in a spherical shell with stress-free boundary condi-

tions and the same Prandtl number as the one used here.

We analyze in detail the stability zones of the primary solutions and we also indicate the characteristics of the most unstable perturbations. The results of the linear stability analysis of the conductive state are again essential. Obtaining η_c is not only critical for elucidating which type of family of modes is the dominant one and what the features of the nonlinear solutions are, but also the proximity of the value of the radius ratio to this point has a profound effect on the shape of the stability regions, as well as on the type of the secondary bifurcation of the primary solutions. Our results show that primary solutions with a radius ratio near η_c are likely to develop double-column convection, whereas primary solutions coming from dominant *normal* modes with a radius ratio sufficiently bigger than η_c, have a tendency to produce vacillating convection.

The model of a fast rotating annulus considered in this paper enables us to study in detail nonlinear convection in a wide range of the values of the parameters, for a fluid of moderate Prandtl number and moderate values of the Rayleigh number. Some of the behavior observed in this paper can also be identified in rotating spherical shells, for example, the generation of strong zonal flows, the tendency to split into multicolumns, or the heat transfer dependence with the Rayleigh number when the Taylor number varies. Thus, we trust that our results may provide some clues about the nonlinear solutions and higher bifurcations associated with the columnar convection in spherical shells.

ACKNOWLEDGMENTS

We are grateful to Dr. Joana Prat for providing a code to calculate the solutions of the problem in the small-gap approximation. We would like to thank DGESIC for supporting this work under Grant No. PB97-0683. D. Pino was supported by a FI grant from the DGR of the Generalitat de Catalunya. Part of the numerical results were obtained by using the CESCA and CEPBA infrastructure coordinated by C^4.

[1] F.H. Busse, Chaos **4**, 123 (1994).
[2] M. Ardes, F.H. Busse, and J. Wicht, Phys. Earth Planet. Inter. **99**, 55 (1997).
[3] F.H. Busse, J. Fluid Mech. **44**, 441 (1970).
[4] K. Zhang, J. Fluid Mech. **236**, 535 (1992).
[5] K. Zhang and F.H. Busse, Geophys. Astrophys. Fluid Dyn. **39**, 119 (1987).
[6] K. Zhang, J. Fluid Mech. **268**, 211 (1994).
[7] A. Tilgner, M. Ardes, and F.H. Busse, Acta Astron. **XIX**, 337 (1997).
[8] F.H. Busse and A.C. Or, J. Fluid Mech. **166**, 173 (1986).
[9] A.C. Or and F.H. Busse, J. Fluid Mech. **174**, 313 (1987).
[10] M. Schnaubelt and F.H. Busse, J. Fluid Mech. **245**, 155 (1992).
[11] N.H. Brummell and J.E. Hart, Geophys. Astrophys. Fluid. Dyn. **68**, 85 (1993).
[12] D. Pino, I. Mercader, and M. Net, Phys. Rev. E **61**(2), 1507 (2000).
[13] A. Tilgner and F.H. Busse, J. Fluid Mech. **332**, 359 (1997).
[14] A.M. Soward, Geophys. Astrophys. Fluid Dyn. **9**, 19 (1977).
[15] A. Alonso, M. Net, and E. Knobloch, Phys. Fluids **7**, 935 (1995).
[16] A. Alonso, M. Net, I. Mercader, and E. Knobloch, Fluid Dyn. Res. **24**, 133 (1998)
[17] A. Alonso, J. Sánchez, and M. Net, Prog. Theor. Phys. Suppl. **139**, 315 (2000).
[18] F. Marques, Phys. Fluids A **2**(5), 729 (1990).
[19] J. Herrmann and F.H. Busse, Phys. Fluids **10**, 1611 (1998).
[20] I. Soibelman and D.I. Meiron, J. Fluid Mech. **229**, 389 (1991).
[21] A. Drissi, M. Net, and I. Mercader, Phys. Rev. E **60**, 1781 (1999).
[22] J. Sánchez and J. Antonijoan, in *Continuation Methods in Fluid Dynamics*, edited by D. Henry and A. Bergeon (Vieweg, Wiesbaden, 2000), Vol. 74, p. 203.
[23] M. Golubitsky, I. Stewart, and D.G. Shaeffer, *Singularities and Groups in Bifurcation Theory* (Springer-Verlag, New York, 1985), Vol. 2.
[24] E. Knobloch, Phys. Fluids **8** (6), 1446 (1996).
[25] I. Mercader, J. Prat, and E. Knobloch, Int. J. Bifurcation Chaos Appl. Sci. Eng. **11**, 27 (2001).
[26] D. Pino, I. Mercader, and M. Net, in *Theory and Tests of Convection in Stellar Structure*, edited by A. Giménez, E.F. Guinan, and B. Montesinos (Astronomical Society of the Pacific Conference Series, San Francisco, 1999), Vol. 173, p. 197.
[27] A.C. Or, J. Fluid Mech. **216**, 613 (1990).
[28] A.C. Or and J. Herrmann, Phys. Fluids **7**(2), 315 (1995).
[29] J. Herrmann and F.H. Busse, J. Fluid Mech. **350**, 209 (1997).